Physics and Chemistry of Minerals (2022) 49:12
https://doi.org/10.1007/s00269-022-01189-3

ORIGINAL PAPER

Equations of state of α-SiC (6H) and β'-$Mg_2Si_{1.1}$ from single-crystal X-ray diffraction data and novel high-pressure magnesium silicide Mg_2Si_7

Iuliia Koemets[1] · Takayuki Ishii[2] · Michael Hanfland[3] · Leonid Dubrovinsky[1]

Received: 20 December 2021 / Accepted: 22 February 2022 / Published online: 3 May 2022

Abstract
SiC and (Fe, Mg)-silicide are candidate phases forming under reducing conditions in the Earth and planetary interiors. However, structural studies of SiC and Mg_2Si at high pressure and their thermal stability are presently lacking. In this work, we applied single-crystal X-ray diffraction in a diamond anvil cell at high pressure and determined the equations of state of α-SiC (6H) and β'-$Mg_2Si_{1.1}$ up to 60 and 40 GPa, respectively, yielding bulk moduli of 226.0(4) and 56(1) GPa. We also report the formation of a novel orthorhombic Mg_2Si_7 phase upon laser heating β'-$Mg_2Si_{1.1}$ at ~ 45 GPa and 2000 °C [*Pbam*, $a = 7.16(1)$ Å, $b = 12.490(3)$ Å, $c = 2.6545(3)$ Å, $V = 237.5(3)$ Å^3]. The structure of this compound contains layers formed by irregular 12-member silicon rings, which are arranged in channels filled with both Mg and Si atoms. No signs of the Mg_2Si_7 phase were detected upon releasing the pressure in the DAC, which suggests that this phase is unstable under ambient conditions.

Keywords Singe-crystal X-ray diffraction · Diamond anvil cell · Magnesium silicide · Silicon carbide

Introduction

Silicon carbide (SiC) is a natural material that has attracted great industrial interest owing to its hardness, refractory, and semi-conductor properties. SiC is commonly found in the Solar System in the form of stardust and chondrite meteorites (e.g., Alexander 1993 and references therein), and has been proposed to potentially constitute a significant volume of planetary interiors in carbon-rich star systems (Madhusudhan et al. 2012). SiC is known as the rare mineral moissanite, which has been reported in bulk kimberlitic chemistry and as inclusions in kimberlitic diamonds (Leung et al. 1990; Shiryaev et al. 2011). Several moissanite grains recovered from ophiolites and kimberlites have been reported to contain inclusions of metallic Si and Fe-silicides (Di Pierro et al. 2003; Trumbull et al. 2009; Shiryaev et al. 2011), and silicides were also found in meteorites (Ross et al. 2019) Because magnesium and silicon are both cosmochemically abundant elements, they are expected to be major components of rocky planets. SiC and (Fe, Mg)-silicide are, therefore, candidates to form Si-bearing minerals under reducing conditions in the Earth and planetary interiors. Additionally, magnesium silicide is considered a promising narrow bandgap semiconductor and has thus been investigated at high pressure in recent years.

SiC_4 tetrahedrons are the main building blocks of SiC crystal structures at ambient pressure. The tetrahedrons are connected at the corners to form layers, and different stacking forms can generate a variety of different SiC polytypes. The most well-studied phases are the zinc-blende type structure (also known as the 3C polytype or β-SiC) and the hexagonal wurtzite-type structure (6H polytype). The 6H polytype together with other hexagonal and rhombohedral structures are also referred to as α-SiC (Shaffer 1969). Previous high-pressure experimental studies have extensively investigated 3C and 6H polytypes using Brillouin spectroscopy

This article is part of a Topical Collection "Experimental & Analytical Techniques at Extreme & Ambient Conditions", guest edited by Stella Chariton, Vitali B. Prakapenka and Haozhe (Arthur) Liu.

✉ Iuliia Koemets
koemets.j@gmail.com

[1] Bayerisches Geoinstitut (BGI), University of Bayreuth, Bayreuth, Germany

[2] Center for High Pressure Science and Technology Advanced Research (HPSTAR), Shanghai, China

[3] European Synchrotron Radiation Facility (ESRF), Grenoble, France

and powder X-ray diffraction (XRD), with reported bulk moduli values of approximately 220–260 GPa (e.g., Daviau and Lee 2018 and references therein). Although some of the reported SiC compressibility data are in reasonable agreement, there remain significant differences in the range of reported observations, as summarized in Table 1. The transition of the 6H-SiC polytype to the rock salt B1-type structure is expected to occur at ~ 100 GPa based on calculations (Eker and Durandurdu 2008). This phase transition is predicted to occur in two stages: 6H-SiC is first compressed along the *c*-direction and then undergoes shear deformation on the *a*-*b* plane. This phase transition was experimentally confirmed during shock compression at ~ 105 GPa (Sekine and Kobayashi 1997). The phase transition of 3C polytype (a cubic structure with three tetrahedral layers) to the same rock salt structure was experimentally observed using powder XRD in a DAC at ambient temperature and ~ 100 GPa (Yoshida and Onodera 1993), and at ~ 60–70 GPa in later works (Miozzi et al. 2018 and references therein). However, studies on crystal structures of SiC and their behaviour at high pressure are presently lacking.

In this work, we studied Mg-bearing silicide endmember. First-principles calculations suggest that cubic Mg_2Si (β-Mg_2Si, anti-fluorite type structure) undergoes a reversible phase transition to an orthorhombic phase at ~ 7 GPa and to a hexagonal polymorph at ~ 20 GPa (Yu et al. 2010). This prediction has been partially confirmed in several experimental studies involving powder diffraction in a DAC using ethanol-methanol (Strössner et al. 1987; Yoshida and Onodera 1993) or NaCl pressure medium (Wang et al. 2016). But the experimental data are largely inconsistent. Cubic Mg_2Si has also been shown to decompose to hexagonal Mg_9Si_5 and Mg at ~ 800 K and 5 GPa (Gaida et al. 2021). Magnesium silicide is usually assumed to have the composition Mg_2Si; however, phase compositions can vary depending on the degree of Mg and Si ordering, which may lead to the formation of different crystal structures.

Here we report the first compressibility study on α-SiC (6H) and β'-$Mg_2Si_{1.1}$ using single-crystal XRD in a diamond anvil cell (DAC) at room temperature up to 60 and 40 GPa, respectively. We also report decomposition of β'-$Mg_2Si_{1.1}$ at high pressure and high temperature. These materials are candidates to form Si-bearing minerals under reducing conditions in the Earth and planetary interiors.

Methods

Sample synthesis

The experimental samples were synthesized using a multi-anvil apparatus. SiC was synthesized using the Iris 1500 ton multi-anvil press with an Osugi-type guide block system at the Bayerisches Geoinstitut (BGI), University of Bayreuth, Germany (Ishii et al. 2016; Ishii et al. 2019). This phase appeared as a side product of phase egg synthesis ($AlSiO_3OH$). The starting material consisted of finely ground $Al(OH)_3$:SiO_2 = 1:1 placed into a welded Pt capsule. The capsule was inserted in a standard BGI 7/3 assembly, compressed to ~ 27 GPa, and then heated to 1300 °C and maintained at this temperature for 3 h. The pressure calibration was conducted in separate runs (Liu et al. 2017) Possible scenarios of carbon contamination in the starting material are as follows. (1) CO_2 may be absorbed from the air during sample storage or preparation. (2) The agate mortar used for sample grinding might be contaminated if previously used with carbonates, even after a thorough cleaning with SiO_2. (3) Carbon may be absorbed from ethanol that did not completely evaporate after sample grinding.

Mg-Si crystals were synthesized from commercial Mg_2Si powder (99.99% metal basis Alfa Aesar) using the Sumitomo 1200 ton multi-anvil press with a split-sphere guide block system at BGI. The pressure calibration was determined in separate runs (Keppler and Frost 2005). The sample was placed into a welded Pt capsule in a standard BGI 10/4 assembly, compressed to ~ 20 GPa, and then heated to ~ 1200 °C and maintained at this temperature for 1 h. The sample was quenched by shutting off the power and then decompressed to ambient pressure.

Table 1 Experimental equations of state for SiC polytypes

Polytype	Maximum pressure (GPa)	EOS	K_0 (GPa)	K_0'	Reference
3C, rock-salt	205	BM EOS	224 (5)	4.1(0.3)	Miozzi et al. (2018)
3C	8.1	BM EOS	237 (2)	4 (fixed)	Wang et al. (2016)
3C, 6H	95	BM EOS	260 (9)	2.9(0.3)	Yoshida and Onodera (1993)
6H	68.4	BM EOS	230 (4)	4 (fixed)	Bassett et al. (1993)
6H	27	BM EOS	218 (5)	4.19 (fixed)	Amulele et al. (2004)
6H	60	BM EOS	226.0 (0.4)	4 (fixed)	This study

All previous studies were conducted using powder diffraction in a diamond anvil cell

BM EOS Burch-Murnaghan equation of state

Sample selection

The recovered crystals were first checked inside a BETSA-type membrane-driven DAC without a pressure medium to ensure that they were pure phases of sufficiently high quality for further experiments. Several crystals were placed in a row inside the DAC and still images were collected by rotating the DAC from − 5° to + 5°. The phases were confirmed by comparing the obtained powder patterns with the patterns generated from CIF files in Dioptas (Prescher and Prakapenka 2015). The crystals with the best reflection quality were chosen for the high-pressure experiments.

High-pressure DAC experiments

We used a BETSA-type membrane-driven DAC with tungsten carbide seats and Boehler-Almax diamonds with 250 or 300 µm culets. Rhenium gaskets were pre-indented to ~ 30 µm thickness, and a hole of approximately 110 µm in diameter was drilled using a SPI RedPower R4 modulated fiber laser (λ ~ 1070 nm) to form a sample chamber. The preselected crystals were then placed in the sample chamber, together with a ruby for pressure determination. The cell was loaded with Ne at the European Synchrotron Radiation Facility (ESRF), Grenoble, France to achieve quasi-hydrostatic conditions during compression. Each DAC was equipped with a steel membrane connected to the helium gas bottle via a pump with a pipe, which allowed the pressure to be remotely controlled within the pressure chamber to achieve desirable pressure steps. During compression, the pressure was determined using the shift of the ruby fluorescence lines (Mao et al. 1986).

Single-crystal X-ray diffraction

Single-crystal XRD data were collected at the ID15B beamline at ESRF. Prior to XRD measurement, the experimental geometry was precisely defined based on a freshly collected diffraction profile from a vanadinite calibrant. The beamline was equipped with a MAR555 flat panel detector for the β'-$Mg_2Si_{1.1}$ experiment, which was upgraded to an Eiger2 X 9 M CdTe detector with dimensions of 340 × 370 mm for the SiC experiment. The operating conditions included an X-ray energy of 30 keV, the wavelength of 0.4133 Å, and beam size of ~ 15 µm at FWHM. Data were collected at each pressure point in the omega range of ± 32°, which was defined by opening the membrane cells (Supplementary Fig. 1, Kantor et al. 2013), using a 0.5° step per frame and exposure time of 1 s per step. The integration of the reflection intensities and absorption corrections were performed using CrysAlis^{Pro} software (Agilent 2014). The structure solution and refinement were carried out using the isotropic approximation in Jana2006 (Petrícek et al. 2014) with Superflip (Palatinus and Chapuis 2007) and SHELXT (Sheldrick 2015).

After compressing β'-$Mg_2Si_{1.1}$ to the maximum pressure, the samples were heated to 2000 K using a double-sided laser heating system at the ID18 beamline at ESRF (Aprilis et al. 2017). Particular care was taken when analyzing the samples after laser heating because the products often became polycrystalline. We first collected a map of still images around the sample by moving the sample stage, and then selected the best spot for data collection where single-crystal reflections (domains) were observed. After processing, reflections of the phase of interest were manually found using the Ewald explorer in CrysAlis^{Pro}; otherwise the data processing routine was similar to that of the unheated samples. Additional experimental detail cold be found in Supplementary Table 1.

Results and discussion

Compressibility of α-SiC (6H)

The structure of the sample studied here consisted of six tetrahedral layers (Fig. 2A, inset) characterized by space group *P63mc* (186) with lattice parameters of $a = 3.0814(8)$ Å, $c = 15.121(2)$ Å, and $V = 124.34(2)$ Å^3, which is indicative of the 6H polytype within the broad class of α-SiC phases (Shaffer 1969).

No phase transitions were observed during the compression of α-SiC (6H) to 60 GPa (Fig. 1A). Reciprocal-space analysis of the SiC crystal at the highest obtained pressure (Fig. 1B) did not reveal any extra reflections or splittings, which confirms that our results are in accordance with the literature data.

Figure 1A shows the unit cell volume as a function of pressure at ambient temperature. Fitting of the pressure–volume data with a second-order Birch-Murnaghan equation of state yields $K_0 = 226.0(4)$ GPa and $V_0 = 124.34(2)$ Å^3, the latter of which was fixed from the experimental data at ambient conditions. A comparison of our result with previous studies (Table 1 after Daviau and Lee (2018) and references therein) demonstrates good agreement with the pioneer high-pressure XRD diffraction study on the 6H polytype by Bassett et al. (1993) and a more recent study by Miozzi et al. (2018). The single-crystal diffraction data collected here in a quasi-hydrostatic pressure medium provide increased accuracy of the bulk modulus determination compared with previous work, and the new results extend the pressure ranges from 8.1 GPa (Wang et al. 2016) and 27 GPa (Amulele et al. 2004) in previous studies to 60 GPa. Our data do not agree with the compressibility reported by Yoshida and Onodera (1993) who studied a mixture of cubic (3C) and hexagonal

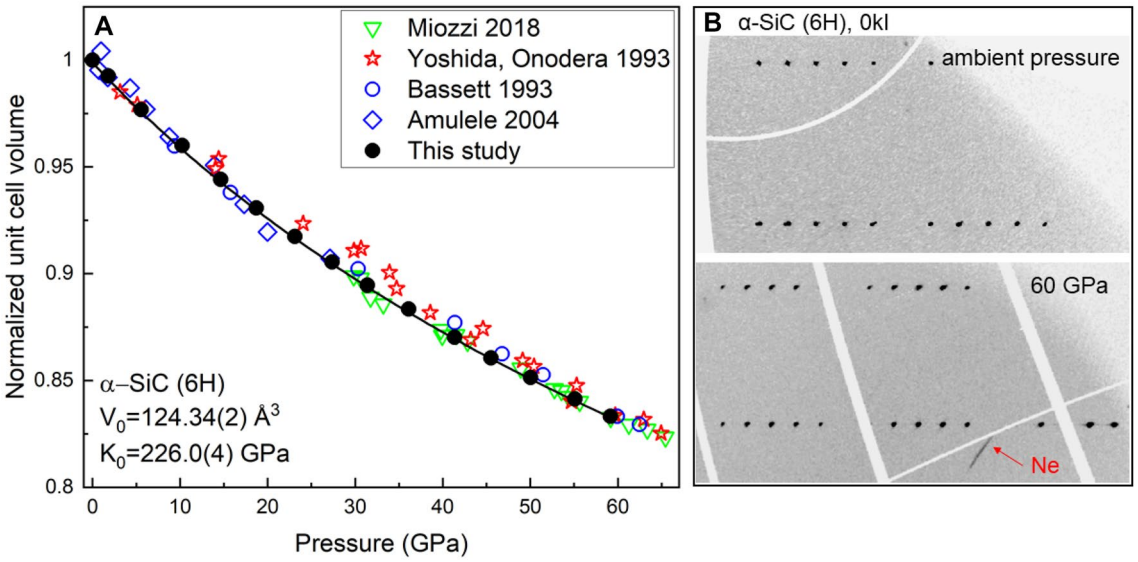

Fig. 1 **A** Equation of state of α-SiC (6H). Black solid curve shows the fit of the experimental data (black circles) with a second-order Birch-Murnaghan equation of state with $V_0 = 124.34(2)$ Å ^{3} and $K_0 = 226.0(4)$ GPa. V_0 was fixed based on the data at ambient conditions. For comparison, we also plot some experimental data for different SiC polytypes (Table 1). See text for discussion. The error bars are within data points **B** Reflections of hexagonal P63mc α-SiC (6H) in the 0kl plane of a precession-like image in reciprocal space reconstructed using the UNWARP procedure within CrysAlis^{Pro} software. As could be observed from the comparison of diffraction image collected at ambient pressure and at ~ 60 GPa, there is no sign of a phase transformation

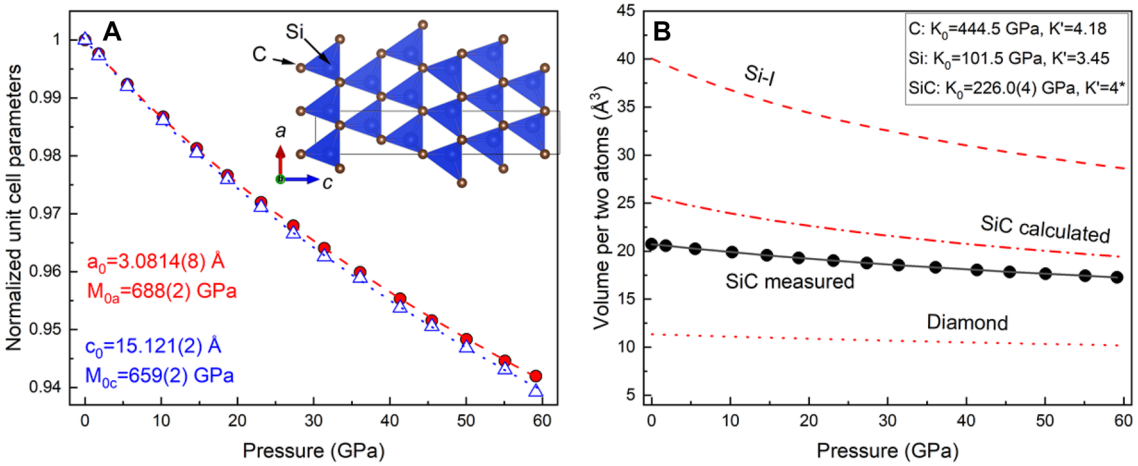

Fig. 2 **A** Normalized unit cell parameters of α-SiC (6H) fitted with a linear second-order Birch-Murnaghan equation of state as a function of pressure. The compressibility is similar along the **a**- and *c*-axes with $M_{0a} = 688(2)$ GPa and $M_{0c} = 659(2)$ GPa. **B** Volume of the SiC formula unit in α-SiC (6H) during compression (black circles, black solid curve). The equations of state for 2C in diamond (red dotted curve) and 2Si in Si-I with the diamond structure (red dashed curve) are plotted for comparison. The red dash-dot curve represents the SiC volume calculated from Si-I and diamond volumes at a given pressure. Note that Si-I is stable only up to ~ 13 GPa. The error bars are within data points

(6H) phases. The long-range order of different polytypes is not expected to cause such a significant difference (~ 40 GPa) of the bulk modulus, thus the discrepancy is likely artificial and may be explained by the different experimental setup, non-hydrostatic conditions, or different pressure calibrants used in that study.

The *c*-axis is found to be slightly more compressible ($M_{0c} = 659(2)$ GPa) than the *a*-axis ($M_{0a} = 688(2)$ GPa) (Figs. 1A, 2). The tetrahedron volume decreased during compression from ~ 3.5 Å^3 at ambient conditions to ~ 3 Å^3 at 50 GPa. The bulk modulus obtained by fitting the SiC_4 tetrahedron volume with a second-order Birch-Murnaghan

equation of state yields $K_0 = 225.7(4)$ GPa, which is indistinguishable from that of the unit cell volume within the experimental uncertainties. The compressibility of bulk 6H-SiC is, therefore, defined by the compressibility of the Si–C bonds. A comparison of the compressibility in diamond (Dewaele et al. 2008) and Si-I with the diamond structure (Anzellini et al. 2019) shows that SiC has a smaller volume than the calculated average Si and C volumes per atom in the unit cells of diamond and Si-I (Fig. 2B). This may indicate that SiC is thermodynamically favorable with respect to a mixture of Si and C over a wide pressure range.

Compressibility of β'-$Mg_2Si_{1.1}$

Computational studies have predicted the phase transitions of Mg_2Si from an anti-fluorite type structure (cubic, *Fm-3 m*) to anti-cotunnite (orthorhombic, *Pmna*) at ~ 6–8 GPa and to a Ni_2In-type structure (hexagonal P63/mmc) at ~ 20–24 GPa (Yu et al. 2010; Huan et al. 2016). In contrast, experimental studies have not been entirely consistent and reports have included the coexistence of anti-cotunnite and Ni_2In-type structured phases (Hao et al. 2009), the presence of hexagonal structures (Cannon and Conlin 1964; Peun et al. 1995), and an unknown monoclinic phase stable above 11.1 GPa (Zhu et al. 2012). This can be explained by the variable chemistry of Mg-Si compounds. Indeed, Huan et al. (2016) computed that Mg_2Si is stable at low and high pressures and is nearly energetically equivalent to hexagonal Mg_9Si_5 at 6–24 GPa.

Several studies have explored the stability of Mg-Si hexagonal phases at high pressure. For example, Ji et al. (2013) synthesized hexagonal Mg_9Si_5 at 5 GPa and 1000 °C [$a = 12.411(1)$ Å, $c = 12.345(1)$ Å, space group $P6_3$], and Gaida et al. (2021) synthesized the same phase at pressures up to 18 GPa and 1200 °C, which is close to our synthesis conditions. Both studies used a mixture of Mg and Si as the starting material.

In this study, we synthesized another Mg-Si hexagonal phase that was recovered after the multi-anvil experiment. The sample is hexagonal with lattice parameters of $a = 7.1554(7)$ Å and $c = 4.1362(7)$ Å, which correspond to previously reported β'-$Mg_2Si_{1.1}$ that has been observed during the precipitation hardening of Al–Mg–Si alloys (Andersen et al. 1998; Vissers et al. 2007). In this structure, Si atoms partly occupy edge positions, two Si atoms are located inside the unit cell at (2/3, 1/3,1/4), and Mg atoms are placed inside the unit cell and can be described either as one Mg in a fully occupied site or two Mg atoms located close to each other with partial occupation (Fig. 3C). Previous reports on this phase described samples with a needle-like shape and size of 2–200 nm. In contrast, the high-pressure synthesis in a multi-anvil press at 20 GPa and 1200 °C applied in this study facilitated crystal growth up to ~ 10–20 µm in lateral dimensions.

The compression of β'-$Mg_2Si_{1.1}$ up to 40 GPa in a quasi-hydrostatic Ne pressure medium did not result in any phase transformations (Fig. 3). The lattice parameters were accurately determined based on at least 170

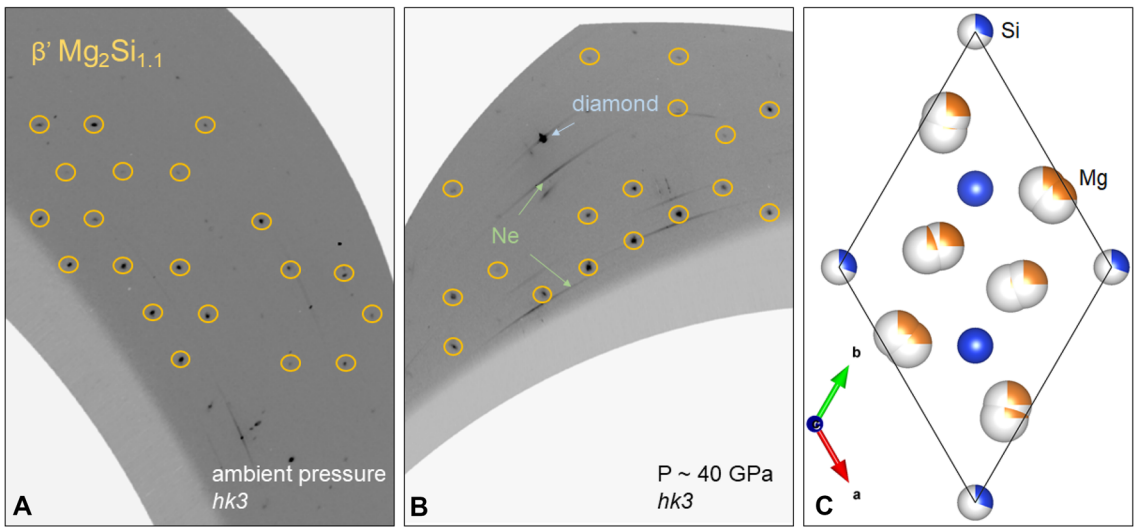

Fig. 3 **A** Reflections of hexagonal β'-$Mg_2Si_{1.1}$ (in yellow circles) in the hk3 plane of a precession-like image of reciprocal space, reconstructed using the UNWARP procedure of CrysAlis^{Pro} software at ambient pressure inside a DAC prior to Ne gas loading, and **B** at ~ 40 GPa. Patterns show no sign of a phase transition, as no new single-crystal reflections are observed. **C** Structure of hexagonal β'-$Mg_2Si_{1.1}$ at ambient conditions. $R_{int} = 5.5\%$, $R_1 = 7.8\%$. Si atoms are marked as blue, Mg atoms are yellow. Atomic positions (x, y, z, occupancy): Si1 (1/3, 2/3, ¼, 1), Si2 [0, 0, 0.3087(10), 0.306(8)], Mg1 [0.6829(9), 0.5970(12), 0.743(7), 0.355(14)), Mg2 (0.730(2), 0.664(3), 0.738(10), 0.145(13)]

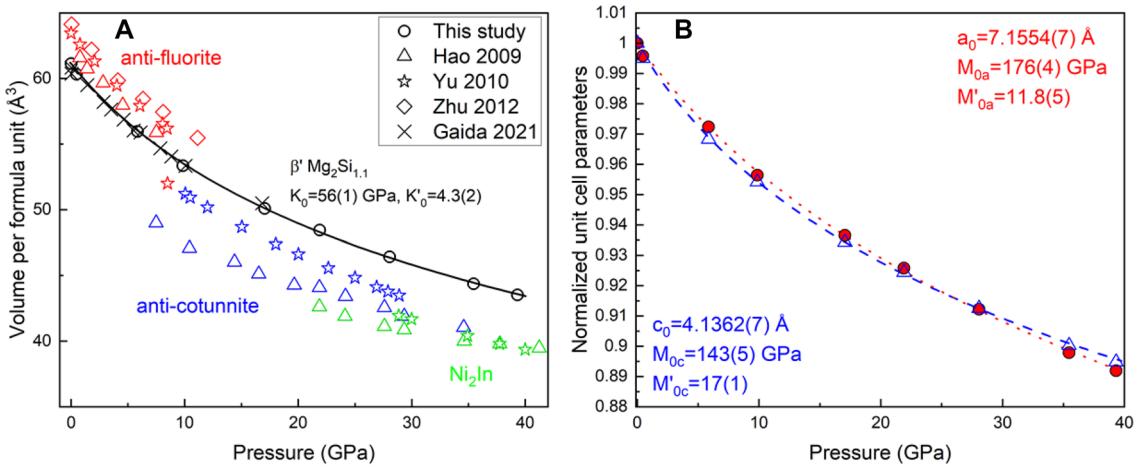

Fig. 4 **A** Compressibility of β'-$Mg_2Si_{1.1}$. Fitting of experimental data (black circles) with a third-order Birch-Murnaghan equation of state (black solid curve) yielding $K_0 = 56(1)$ and $K'_0 = 4.3(2)$. V_0 was fixed based on the data at ambient conditions. For comparison, we show the volume per formula unit for anti-fluorite Mg_2Si (red), anti-cotunnite (blue), and Ni_2In-type Mg_2Si (green), in addition to hexagonal Mg_9Si_5 (black crosses) Data from Yu et al. (2010) are based on calculations. **B** Normalized unit cell parameters of β'-Mg-Si as a function of pressure. The error bars are within data points

single-crystal reflections, showing a monotonic and anomaly-free decrease with pressure (Fig. 4A). However, a refinement of the atomic coordinates was not feasible owing to the structure complexity and limited diffraction data quality. These observations deviate from the previously reported high-pressure behavior of stoichiometric Mg_2Si, which undergoes multiple phase transitions in the pressure range up to 40 GPa (Fig. 4A).

Fitting the pressure–volume data for β'-$Mg_2Si_{1.1}$ with a third-order Burch-Murnaghan equation of state yields $K_0 = 56(1)$ GPa, $K' = 4.3(2)$, and $V_0 = 183.40(4)$ Å^3 (Supplementary Fig. 2). The compressibility of β'-$Mg_2Si_{1.1}$ is therefore similar to that of cubic anti-fluorite Mg_2Si ($K_0 = 57.03(2)$ GPa, $K' = 4$ (fixed), $V_0 = 62.34(1)$ Å^3; Hao et al. 2009). Our data are also in good agreement with the compressibility of hexagonal Mg_9Si_5 recently reported by Gaida et al. (2021) [$K_0 = 58(3)$ GPa, $K' = 4.1(7)$, $V_0 = 1643(2)$ Å^3].

The reported bulk moduli of Mg_2Si high-pressure phases are significantly higher than that determined here for β'-$Mg_2Si_{1.1}$. For example, anti-cotunnite Mg_2Si has $K_0 = 102.65(5)$ and Ni_2In-type Mg_2Si has $K_0 = 163.83(10)$ (Hao et al. 2009). We demonstrate that β'-$Mg_2Si_{1.1}$ does not undergo phase transitions as does cubic Mg_2Si, and is considerably more compressible than the high-pressure forms of the latter phase. There are several possible reasons for this divergent behavior: (1) different transformational pathways for different starting materials, which is a well-known phenomenon in silicon dioxide (Bykova et al. 2018); (2) differing chemical compositions of the materials (i.e. Mg/Si ratio); and (3) different experimental conditions, particularly the hydrostaticity of the pressure medium. Our results thus highlight the need for further investigation of Mg_2Si polymorphs at high pressure using modern single-crystal X-ray diffraction methods.

Decomposition of β'-$Mg_2Si_{1.1}$ at high temperature and novel Mg_2Si_7

After laser heating to 2000 K at ~ 45 GPa, β'-$Mg_2Si_{1.1}$ decomposed and formed a novel Mg_2Si_7 phase (Figs. 4, 5), which is orthorhombic (*Pbam*, 55) with $a = 7.16(1)$ Å, $b = 12.490(3)$ Å, $c = 2.6545(3)$ Å, and $V = 237.5(3)$ Å^3. The structure of this phase was solved and refined to $R_1 = 0.08$ based on 96 reflections (see supplementary CIF file). Even if the X-ray scattering factors of Mg and Si are similar, the quality of the diffraction data allows an unambiguous assignment of the structural positions to determine the composition of the phase as Mg_2Si_7.

The remarkable features of this phase include its layered structure, which consists of layers formed by irregular 12-member silicon rings. The rings are arranged in channels filled with both Mg and Si atoms (Fig. 5). The bond length of the Si–Si forming channels is ~ 2.55 Å. The distance from a Si atom inside the channel to the closest Si atom is ~ 2.61 Å. A comparison of the known bond lengths at ambient conditions show that this bond length is substantially larger than the double Si–Si bond length

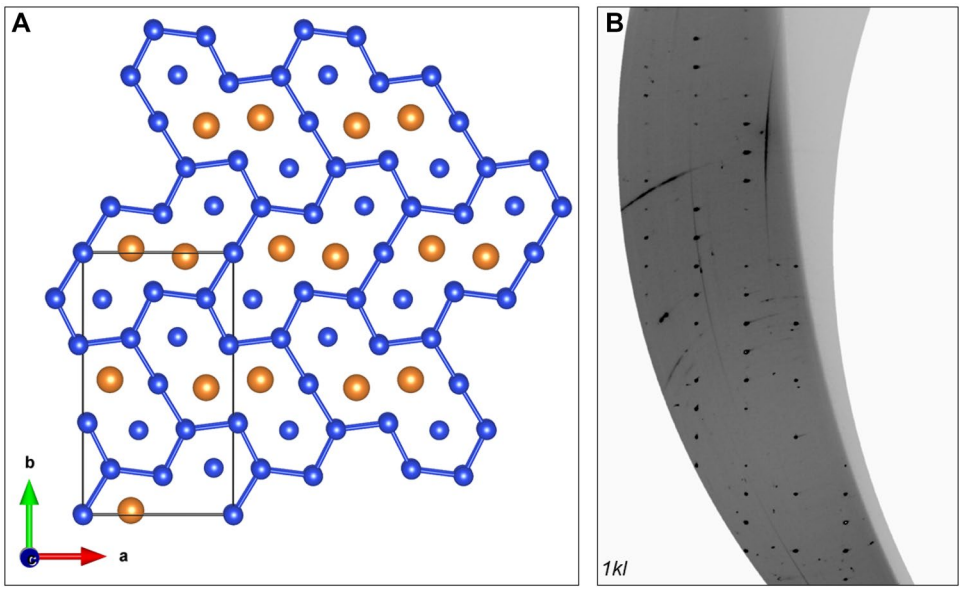

Fig. 5 **A** Novel high-pressure Mg_2Si_7 phase. A Z-shaped framework with Si atoms creates infinite channels filled with Mg and Si atoms. Space group Pbam, (55) with $a = 7.16(1)$ Å, $b = 12.490(3)$ Å, $c = 2.6545(3)$ Å, and $V = 237.5(3)$ Å^3. VESTA software was used to generate the structure image. **B** Reflections of the novel Mg_2Si_7 phase synthesized after laser heating to ~ 2000 K in the 1kl plane of a precession-like image of reciprocal space. From the reflections arrangement in comparison with Fig. 3A and B one could note, that hexagonal $Mg_2Si_{1.1}$ transformed to the phase with orthorhombic symmetry

in silenes (~ 2.14 Å) and normal Si–Si bonds (~ 2.3 Å), but also shorter than the longest known Si–Si σ bond (~ 2.7 Å) and recently reported single π bond (~ 2.8 Å) (Kyushin et al. 2020). The obtained distance is similar to that between atoms in neighboring hexagonal layers of hcp Si in high-pressure Si polymorphs (2.5344 Å at 42.5 GPa; Hanfland et al. 1999)) and in hexagonal Mg_9Si_5 (~ 2.5 Å; Gaida et al. 2021). The Mg-Mg distance in the novel Mg_2Si_7 structure is ~ 2.61–2.65 Å, which is significantly shorter than that in Mg_9Si_5 (3.1 Å). The shortest Mg-Si distance in the novel Mg_2Si_7 phase is ~ 2.6 Å, which is longer than that in Mg_9Si_5 (2.42 Å). The Si atoms located inside the channels are 12-fold coordinated with Si chain-forming atoms and an average bond length ~ 2.7 Å.

No signs of the Mg_2Si_7 phase were detected upon releasing the pressure in the DAC, which suggests that this phase is unstable at ambient conditions.

As silicides are known in meteorites, and magnesium and silicon are cosmochemically abundant elements, one can hypothesize magnesium silicide(s) (or solid solutions based on Mg-Si phases) may be present in the interior of reduced rocky planets. Our results suggest that the high-pressure behavior of Mg-Si is complex and warrant further investigations.

Conclusions

We report the equations of state for α-SiC (6H) up to 60 GPa based on high-precision single-crystal XRD in a DAC. We also studied the compressibility of β'-$Mg_2Si_{1.1}$ up to 40 GPa and report a novel Mg_2Si_7 structure consisting of layers formed by irregular 12-member silicon rings that contain channels filled with both Mg and Si atoms.

Supplementary Information The online version contains supplementary material available at https://doi.org/10.1007/s00269-022-01189-3.

Funding Open Access funding enabled and organized by Projekt DEAL.

Declarations

Conflict of interest The authors declare that they have no conflict of interest. I.K and L.D. were funded by DFG 939/9-2 and DFG 939/13-2.

References

Agilent (2014) CrysAlisPro data collection and processing software for Agilent X-ray diffractometers. CrysAlis PRO. Agilent Technologies Ltd, Yarnton, Oxfordshire England

Alexander CMO (1993) Presolar SiC in chondrites: how variable and how many sources? Geochim Cosmochim Acta 57(12):2869–2888. https://doi.org/10.1016/0016-7037(93)90395-D

Amulele GM et al (2004) High pressure ultrasonic and x-ray studies on monolithic SiC composite. J Appl Phys 95(4):1806–1810. https://doi.org/10.1063/1.1639141

Andersen SJ et al (1998) The crystal structure of the β'' phase in Al-Mg-Si Alloys. Acta Mater 46(9):3283–3298. https://doi.org/10.1016/S1359-6454(97)00493-X

Anzellini S et al (2019) Quasi-hydrostatic equation of state of silicon up to 1 megabar at ambient temperature. Sci Rep. Springer, US 9(1):1–14. https://doi.org/10.1038/s41598-019-51931-1

Aprilis G et al (2017) Portable double-sided pulsed laser heating system for time-resolved geoscience and materials science applications. Rev Sci Instrum. https://doi.org/10.1063/1.4998985

Bassett WA et al (1993) Compressibility of SiC up to 68.4 GPa. J Appl Phys 74(6):3824–3826. https://doi.org/10.1063/1.354476

Bykova E et al (2018) Metastable silica high pressure polymorphs as structural proxies of deep Earth silicate melts. Nat Commun 9(1):4789. https://doi.org/10.1038/s41467-018-07265-z

Cannon F, Conlin ET (1964) Magnesium compounds: new dense phases. Science 145(3631):487–489. https://doi.org/10.1126/science.145.3631.487

Daviau K, Lee KKM (2018) High-pressure, high-temperature behavior of silicon carbide: a review. Curr Comput-Aided Drug Des 8(5):1–18. https://doi.org/10.3390/cryst8050217

Dewaele A et al (2008) High pressure-high temperature equations of state of neon and diamond. Phys Rev B-Condens Matter Mater Phys 77(9):1–9. https://doi.org/10.1103/PhysRevB.77.094106

Di Pierro S et al (2003) Rock-forming moissanite (natural α-silicon carbide). Am Miner 88:1817–1821. https://doi.org/10.7892/boris.86644

Eker S, Durandurdu M (2008) Phase transformation of 6H-SiC at high pressure: an ab initio constant-pressure study. EPL. https://doi.org/10.1209/0295-5075/84/26003

Gaida NA et al (2021) Phase relations and thermoelasticity of magnesium silicide at high pressure and temperature. J Chem Phys. https://doi.org/10.1063/5.0044648

Hanfland M et al (1999) Crystal structure of the high-pressure phase silicon vi. Phys Rev Lett 82(6):1197–1200. https://doi.org/10.1103/PhysRevLett.82.1197

Hao J et al (2009) In situ X-ray observation of phase transitions in Mg2Si under high pressure. Solid State Commun 149(17–18):689–692. https://doi.org/10.1016/j.ssc.2009.02.018

Huan TD et al (2016) High-pressure phases of Mg2Si from first principles. Phys Rev B 93(9):1–7. https://doi.org/10.1103/PhysRevB.93.094109

Ishii T et al (2016) Generation of pressures over 40 GPa using Kawai-type multi-anvil press with tungsten carbide anvils. Rev Sci Instrum 87(2):2–8. https://doi.org/10.1063/1.4941716

Ishii T, Liu Z, Katsura T (2019) A breakthrough in pressure generation by a Kawai-type multi-Anvil apparatus with tungsten Carbide Anvils. Engineering 5:434–440. https://doi.org/10.1016/j.eng.2019.01.013

Ji S et al (2013) Structural characterization of magnesium-based compounds Mg9Si5 and Mg4Si3Al (superconductor) synthesized under high pressure and high temperature conditions. Inorg Chem 52:3953–3961. https://doi.org/10.1021/ic3027539

Kantor I et al (2012) BX90: a new diamond anvil cell design for X-ray diffraction and optical measurements. Rev Sci Instrum. 83:125102. https://doi.org/10.1063/1.4768541

Keppler H, Frost DJ (2005) Introduction to minerals under extreme conditions. In: Miletich R (ed) EMU notes in mineralogy. Mineralogical society of Great Britain and Ireland, London, pp 1–30. https://doi.org/10.1180/EMU-notes.7

Kyushin S et al (2020) Silicon–silicon π single bond. Nat Commun 11(1):1–7. https://doi.org/10.1038/s41467-020-17815-z

Leung I et al (1990) Natural occurrence of silicon carbide in a diamondiferous kimberlite from Fuxian. Nature 346(6282):352–354. https://doi.org/10.1038/346352a0

Liu Z et al (2017) Phase relations in the system MgSiO3-Al2O3 up to 2300 K at lower mantle pressures. J Geophys Res : Solid Earth 122(10):7775–7788. https://doi.org/10.1002/2017JB014579

Madhusudhan N, Lee KKM, Mousis O (2012) A possible carbon-rich interior in super-earth 55 cancri e. Astrophys J Lett. https://doi.org/10.1088/2041-8205/759/2/L40

Mao HK, Xu J, Bell PM (1986) Calibration of the ruby pressure gauge to 800 kbar under quasi-hydrostatic conditions. J Geophys Res 91(B5):4673–4676

Miozzi F et al (2018) Equation of state of SiC at extreme conditions: new insight into the interior of carbon-rich exoplanets. J Geophys Res: Planets 123(9):2295–2309. https://doi.org/10.1029/2018JE005582

Palatinus L, Chapuis G (2007) SUPERFLIP—a computer program for the solution of crystal structures by charge flipping in arbitrary dimensions. J Appl Crystallogr 40(4):786–790. https://doi.org/10.1107/S0021889807029238

Petrícek V, Dušek M, Palatinus L (2014) Crystallographic computing system JANA2006: general features. Zeitschrift Kristallogr 229(5):345–352. https://doi.org/10.1515/zkri-2014-1737

Peun T, Lauterjung J, Hinze E (1995) High pressure and high temperature investigations on intermetallic compounds using energy-dispersive X-ray powder diffraction. Nucl Instrume Methods Phys Res, B 97:483–486. https://doi.org/10.1016/0168-583X(94)00358-0

Prescher C, Prakapenka VB (2015) DIOPTAS: A program for reduction of two-dimensional X-ray diffraction data and data exploration. High Press Res 35(3):223–230. https://doi.org/10.1080/08957959.2015.1059835

Ross AJ et al (2019) The origin of iron silicides in ureilite meteorites. Geochemistry. https://doi.org/10.1016/j.chemer.2019.125539

Sekine T, Kobayashi T (1997) Shock compression of 6H polytype SiC to 160 GPa. Phys Rev B 55(13):8034–8037. https://doi.org/10.1103/PhysRevB.55.8034

Shaffer PTB (1969) 'A review of the structure of silicon carbide. Acta Crystallogr Sect b: Int Union Crystallogr 25(3):477–488. https://doi.org/10.1107/s0567740869002457

Sheldrick GM (2015) 'SHELXT—integrated space-group and crystal-structure determination. Acta Crystallogr Sect a: Found Crystallogr: Int Union Crystallogr 71(1):3–8. https://doi.org/10.1107/S2053273314026370

Shiryaev AA, Griffin WL, Stoyanov E (2011) Moissanite (SiC) from kimberlites: polytypes, trace elements, inclusions and speculations on origin. Lithos 122(3–4):152–164. https://doi.org/10.1016/j.lithos.2010.12.011

Strössner K, Cardona M, Choyke WJ (1987) High pressure X-ray investigations on 3C-SiC. Solid State Commun 63(2):113–114. https://doi.org/10.1016/0038-1098(87)91176-8

Trumbull RB et al (2009) The carbon isotope composition of natural SiC (moissanite) from the Earth ' s mantle : new discoveries from ophiolites. Lithos 113(3–4):612–620. https://doi.org/10.1016/j.lithos.2009.06.033

Vissers R et al (2007) The crystal structure of the β' phase in Al-Mg-Si alloys. Acta Mater 55(11):3815–3823. https://doi.org/10.1016/j.actamat.2007.02.032

Wang Y et al (2016) Thermal equation of state of silicon carbide. Appl Phys Lett. https://doi.org/10.1063/1.4941797

Yoshida M, Onodera A (1993) Pressure-induced phase transition in SiC. Phys Rev B 48(14):1–5. https://doi.org/10.1007/s00894-015-2852-5

Yu F et al (2010) A study of the phase transitions, electronic structures and optical properties of Mg2Si under high pressure. Solid State Commun 150(13–14):620–624. https://doi.org/10.1016/j.ssc.2009.12.031

Zhu F et al (2012) A re-investigation on pressure-induced phase transition of Mg2Si. Solid State Commun. Elsevier 152(24):2160–2164. https://doi.org/10.1016/j.ssc.2012.09.015